PCCP

ROYAL SOCIETY OF CHEMISTRY

PAPER

View Article Online
View Journal | View Issue

Cite this: *Phys. Chem. Chem. Phys.*, 2023, **25**, 20892

Room temperature epoxidation of ethylene over delafossite-based $AgNiO_2$ nanoparticles†

Dmitry A. Svintsitskiy,* Mikhail K. Lazarev, Elena M. Slavinskaya, Elizaveta A. Fedorova, Tatyana Yu. Kardash, Svetlana V. Cherepanova and Andrei I. Boronin

Received 14th April 2023,
Accepted 15th July 2023

DOI: 10.1039/d3cp01701j

rsc.li/pccp

A mixed oxide of silver and nickel $AgNiO_2$ was obtained *via* co-precipitation in alkaline medium. This oxide demonstrates room temperature activity in the reaction of ethylene epoxidation with a high selectivity (up to 70%). Using the PDF method, it was found that the initial structure of $AgNiO_2$ contains stacking faults and silver vacancies, which cause the nonstoichiometry of the oxide (Ag/Ni < 1). It has been established that on the initial surface of $AgNiO_2$ oxide, silver state can be considered as an intermediate between Ag_2O and Ag^0 (*i.e.* $Ag^{\delta+}$-like), while nickel is characterized by signs of a deeply oxidized state (Ni^{3+}-like). The interaction of $AgNiO_2$ with C_2H_4 at room temperature leads to the simultaneous removal of two oxygen species with E_b(O 1s) = 529.0 eV and 530.5 eV considered as nucleophilic and electrophilic oxygen states, respectively. Nucleophilic oxygen was attributed to the lattice oxygen (Ag–O–Ni), while the electrophilic species with epoxidation activity was associated with the weakly bound oxygen stabilized on the surface. According to the TPR-C_2H_4 data, a large number of weakly bound oxygen species were found on the pristine $AgNiO_2$ surface. The removal of such species at room temperature didn't result in noticeable structural transformation of delafossite. As the temperature of ethylene oxidation over $AgNiO_2$ increased, the appearance of Ag^0 particles was first observed below 200 °C followed by the complete destruction of the delafossite structure at higher temperatures.

Introduction

The development of efficient and low-cost catalytic systems is an urgent task for new and promising chemical industries. In exploratory studies, special attention is paid to catalysts that do not contain expensive precious metals or whose content is significantly reduced compared to the commonly used catalysts. In oxidative catalysis, there is interest in mixed oxides where oxygen is coordinated by different metal ions (*e.g.*, M1–O–M2), which causes significant modification of the electronic structure and reactive properties.[1–3] Among the relevant characteristics of mixed oxides providing potential application in selective oxidation reactions the next ones must be mentioned: the multifunctionality of the surface sites, a moderate bond strength of the active oxygen, and the high RedOx ability of the catalyst.[4] Therefore, mixed oxides of transition metals should be regarded as efficient and inexpensive alternative catalytic systems for various oxidative processes.

Among the variety of mixed oxides, it is worth highlighting systems with a delafossite-type structure with the general composition ABO_2, where A is a monovalent metal cation (usually Ag^{1+} or Cu^{1+}), and B is a trivalent metal cation (Fe^{3+}, Co^{3+}, Al^{3+}, *etc.*[5]) or various combinations of low- and high-valent forms (M^{2+}/M^{4+},[6] M_2^{2+}/M^{5+}[1]). The delafossite and related crednerite structure types are described in detail elsewhere.[7,8] The potential of delafossite-type materials in the field of oxidative catalysis is high due to several reasons: (1) the presence in composition of Cu^{1+} or Ag^{1+} ions for activation of the O_2 molecule;[9] (2) point and extended defects providing additional active sites;[10,11] (3) the possibility for optimization of the RedOx properties by selecting the B cation and/or doping.[12] The properties considered agree well with the presence of highly reactive oxygen forms capable of interacting with reactants at low temperatures as was observed for silver-containing mixed oxides.[13,14] It was found that the high oxidative activity of the $AgNiO_2$ oxide with the delafossite-type structure is ensured not only by the lattice oxygen (Ag–O–Ni), but also by an additional weakly charged form,[14] which is of interest for the selective oxidation reactions.

Traditionally, silver-containing catalysts are used in various selective oxidation processes, including ethylene epoxidation.[15–19]

Boreskov Institute of Catalysis, Pr. Lavrentieva 5, 630090, Novosibirsk, Russian Federation. E-mail: sad@catalysis.ru

† Electronic supplementary information (ESI) available. See DOI: https://doi.org/10.1039/d3cp01701j

Despite a large amount of experimental and theoretical data obtained using modern physicochemical methods, the nature of active and selective oxygen species and their electronic structure on the surface of silver particles is still the subject of debate.[15,20–24] It is well established that the silver surface is reconstructed (at least partially) due to the oxidation under the conditions of the epoxidation reaction.[21,25] It is believed that the epoxidation activity of silver is associated with the stabilization of weakly charged oxygen (E_b(O 1s) > 530 eV) on its surface, which is known as electrophilic oxygen.[26–30] Nucleophilic oxygen with E_b(O 1s) < 529 eV, necessary for the adsorption and activation of the ethylene molecule, is able to break the C–H bond and, therefore, lead to the complete oxidation of ethylene.[25,29,31,32] The nucleophilic species usually include lattice (Ag_2O-like) and near-surface atomic oxygen, which causes the stabilization of oxidized silver.[23,29,30] In recent works, using *in situ* physicochemical methods, it has been shown that molecular and hybrid species stabilized on defects of silver particles should be considered as electrophilic oxygen directly involved in the epoxidation of ethylene.[20–23]

Although traditional silver catalysts are usually metal particles on the surface of the oxide support (*e.g.*, Al_2O_3),[22] silver-containing mixed oxides are also used in selective oxidative reactions, including epoxidation. For example, a composite catalyst based on $AgFeO_2$ oxide with a delafossite structure demonstrated promising performance in cycloalkene epoxidation reactions (selectivity in the range of 70–100% at a conversion of at least 23%).[33] The catalytic measurements of $Ag_2Cu_2O_3$ mixed oxide caused the destruction of the initial structure with the formation of an Ag^0/CuO composite under the ethylene oxidation reaction.[34] However, the resulting composite showed activity in the epoxidation of ethylene (selectivity above 10% at a conversion close to 10%). Another mixed oxide (Ag_2CuMnO_4) with the delafossite structure showed catalytic characteristics close to those of $Ag_2Cu_2O_3$ in the ethylene oxidation reaction without bulk destruction up to 200 °C.[35] It was also shown that a mixed oxide of copper and titanium $TiCuO_x$ with an unknown structure, is capable of direct epoxidation of propylene.[36] Obviously, the epoxidation activity of mixed oxides or metal-oxide composites formed during their destruction is associated with the stabilization, as in the case of silver catalysts, of specific forms of active oxygen. The nature and state of metals in the mixed oxides, as well as their structure, play an important role in the stabilization of such forms. Mixed oxides with the delafossite structure are characterized by a variety of possible point and extended defects,[10,11] which determines the interest in their application in the both total and selective oxidation reactions.

In this work, nanoparticles of mixed oxide $AgNiO_2$ were tested in the ethylene oxidation reaction. It has been found that the $AgNiO_2$ surface contains oxygen species capable of efficiently converting ethylene to ethylene oxide (EtO) at room temperature with selectivity close to 70%. The appearance of such forms is associated with s states of silver and nickel on the $AgNiO_2$ surface.

Experimental part

Synthesis

$AgNiO_2$ samples were prepared by co-precipitation in an alkaline medium (NaOH) in the presence of $Na_2S_2O_8$ using $AgNO_3$ and $Ni(NO_3)_2{\cdot}6H_2O$ as initial reagents.[14] Dropping a solution of nitrates into an alkaline solution of $Na_2S_2O_8$ resulted in the formation of a black precipitate. The precipitate was aged in the mother liquor for 1 h at 90 °C. Then, it was filtered and washed with distilled water, followed by drying for 4 h at 90 °C in air. Preparation of Ag_2O, Ag^0, NiO, and $Ni(OH)_2$ standard samples is described in the ESI.†

Physicochemical study

The diffraction patterns were obtained using a Bruker D8 diffractometer (Germany) and CuKα-radiation (λ = 0.154184 nm). Measurements were carried out with a one-dimensional LynxEye detector and Bragg–Brentano focusing. The signal was recorded in the 2θ range from 15 to 90° (0.05° step, counting time 3 s). *In situ* XRD patterns were obtained using an Anton Paar XRK900 reaction camera (Austria) in a flow of reaction gas, which was supplied at a rate of 70 mL min^{-1}. The ICDD PDF-2 database was used for phase analysis.

The photoelectron spectra were acquired using the AlKα line ($h\nu$ = 1486.6 eV) on a VG ESCALAB HP spectrometer. The instrument was calibrated using the binding energies of the Au $4f_{7/2}$ (84.0 eV) and Cu $2p_{3/2}$ (932.7 eV) peaks for bulk gold and copper foils, respectively. The spectra were processed (smoothing, curve-fitting, and calculation of peak areas) using the "XPS-Calc" program applied earlier for various systems.[37–39] The curve-fitting was carried out with the approximation of the peaks by the sum of the Lorentz and Gauss functions with the subtraction of the background by the Shirley method. The spectra are presented after normalization to the area of the Ni 2p line. To plot the O 1s difference spectra, normalization was performed to the total content of Ag and Ni on the surface. The ratios of elements on the surface were determined using atomic sensitivity factors (ASF), the calculation details of which are presented in the ESI.†

Diffraction data for PDF (Pair Distribution Function) analysis were obtained using synchrotron radiation at ESRF, ID15b station (Grenoble, France) equipped with a two-dimensional PilatusX CdTe detector. The wavelength (λ) of monochromatic radiation was 0.142774 Å, which was refined using the CeO_2 standard sample. The integration was carried out using the pyFAI program.[40] The normalized scattering curves $S(Q)$ and the corresponding PDF curves ($G(r)$) were calculated from the intensity curve using the PDFgetX3 program[41] (eqn (1)):

$$G_{\exp}(r) = \frac{2}{\pi}\int_{Q_{\min}}^{Q_{\max}} Q[S(Q) - 1]\sin(Qr)\mathrm{d}Q = 4\pi[\rho(r) - \rho_0] \quad (1)$$

where $Q = 4\pi \sin\Theta/\lambda$ is the scattering vector. The upper integration limit was $Q_{\max}$ = 29 $Å^{-1}$, $\rho(r)$ is pair atomic density (probability of finding atom i at a distance r from atom j), ρ_0 – average density. PDF simulation was performed in PDFgui[42]

according to eqn (2):

$$G_{\text{calc}}(r) = \frac{1}{r}\sum_i \sum_j \left[\frac{f_i f_j}{\langle f\rangle^2}\delta(r - r_{ij})T_{ij}(r)\right] - 4\pi r\rho_0 \qquad (2)$$

where r is the interatomic distance, f_i is the atomic scattering of atom i, and $T_{ij}(r)$ is the temperature factor, which takes into account individual thermal vibrations of atoms, correlated thermal vibrations, and diffractometer resolution.

The specific surface area was determined from low-temperature nitrogen adsorption and calculated according to the BET theory.[43] Nitrogen adsorption isotherms were measured at 77 K on a QUADRASORB evo adsorption analyzer (Quantachrome Instruments, USA) after preliminary degassing at 120 °C using a FloVac degasser.

Catalytic and reaction properties

The catalytic properties were studied by temperature-programmed reaction (TPR) using an automated setup equipped with a flow reactor and an RGA-200 quadrupole mass spectrometer (SRS, USA) for analyzing the reaction mixture. The sample (weight of 0.9 g, fraction 0.14–0.25 mm) was loaded into the reactor, and the reaction mixture was introduced at 25 °C (space velocity of 100 $cm^3\ min^{-1}$). The reaction mixture contained 2.5 vol% C_2H_4, 5 vol% O_2, and 0.5 vol% Ne (in He). To identify ethylene oxidation products, MS signals with m/z values of 15 and 20 (signal from Ne), as well as 25, 41, 42, and 44 were recorded. Other details of MS quantification are presented in the ESI.† Ethylene and its oxidation products (C_2H_4O, CO_2, CH_3CHO) were quantified using matrix analysis based on different contributions for selected m/z values.[44] To carry out the temperature-programmed reduction by ethylene (TPR-C_2H_4), the sample weight was 0.2 g, the volumetric flow rate was 1000 $cm^3\ min^{-1}$, and the reaction mixture contained 1 vol% C_2H_4, 0.5 vol% Ne (in He), and a heating rate of 10 °C min^{-1}. A TPO study was performed using a mixture of 1 vol% O_2, and 0.5 vol% Ne (in He) supplied with a space velocity of 100 $cm^3\ min^{-1}$. Before the TPO experiment, $AgNiO_2$ was treated with a mixture of 2.5%C_2H_4/0.5%Ne/He at 30 °C for more than 1 h.

Results

Structure characterization

Mixed oxide $AgNiO_2$ obtained by co-precipitation has been partially characterized in our previous work.[14] As a result of the synthesis, highly dispersed $AgNiO_2$ particles with a delafossite structure and a specific surface area of 80–100 $m^2\ g^{-1}$ were formed (Fig. S1, ESI†). Fig. 1a shows the PDF curve for the initial sample of $AgNiO_2$. The peaks on the curve qualitatively corresponded to the interatomic distances in the delafossite structure. It should be noted that there are two polytypes of the delafossite structure (2H and 3R), which differ in the way of stacking of brucite layers that are built from NiO_6 sharing edges octahedra. Both polytypes have the same structure of brucite layers, while the interatomic distances that correspond to the stacking of the layers differ (Fig. 1b). When the 3R polytype structure was used to describe experimental PDF data, the peaks corresponding to interatomic distances with $r < 5$ Å were described well, while the peaks at large distances were described unsatisfactorily (Fig. 1a). This deviation is typical for structures with a high concentration of stacking faults, for instance, CdSe nanoparticles.[45] The interlayer distances in the delafossite structure are greater than 5 Å, for which the greatest deviation of the calculated and experimental PDF curves is observed.

Since stacking faults often arise during the formation of nanoparticles with a delafossite-type layered structure,[10,46] we have considered such defects for $AgNiO_2$. To simulate the defect structure, a super-cell consisting of 8 layers was constructed, where two types of layer stacking characteristic to 2H and 3R polytypes were presented in equal proportion (Fig. 1b). The resulting model was refined with respect to the experimental PDF data (Fig. 1c). A much better description of the experimental data was achieved (R-factor of 0.25) than in the case of the 3R polytype structure only (R = 0.32, Fig. 1a). Model calculations of the diffraction pattern by varying the probability of the appearance of 3R polytype layers also showed that the best agreement with the experimental diffraction pattern is achieved for a model with 50% probability of the appearance of a 3R layer (Fig. S2, ESI†).

The description of the experimental PDF curve using a defect structure was additionally improved by taking into account the temperature parameter, which describes the average displacements of silver atoms along the c axis (direction of layer stacking). Also, vacancies in the silver positions were introduced. As a result, the R factor dropped from 0.25 to 0.22 (Fig. 1b). The structural parameters obtained by refinement for the $AgNiO_2$ defect model are given in Table S1 (see the ESI†). Note that, according to the X-ray fluorescence data, the Ag/Ni ratio in the initial sample was close to 0.8. According to the XPS data for different pristine samples, the Ag/Ni surface ratio varied in the range from 0.7 to 0.9, which confirms the depletion of the $AgNiO_2$ structure with silver, which is probably the most pronounced for the particle surface.

Thus, the $AgNiO_2$ oxide prepared by co-precipitation in an alkaline medium was characterized by the defect delafossite structure. The obtained dispersed particles have a high concentration of stacking faults, when NiO_6 brucite layers are stacked according to 2H or 3R structure-type with similar probability. In this case, disordering of the silver positions (large displacements along the c direction) and vacancies in these positions (Ag/Ni < 1) occur.

X-ray photoelectron spectroscopy (XPS)

The electronic state of elements on the surface of $AgNiO_2$ oxide was studied by XPS and compared with data for standard samples and literature.[14,47,48] The appearance of Ni^{3+} forms is usually confirmed by the presence of low-intensity shake-up satellites of the Ni 2p line simultaneously with a high value of binding energy (E_b) for the Ni $2p_{3/2}$ peak ($\geq$856 eV).[49,50] Note that this peak is also observed for pure NiO and $Ni(OH)_2$

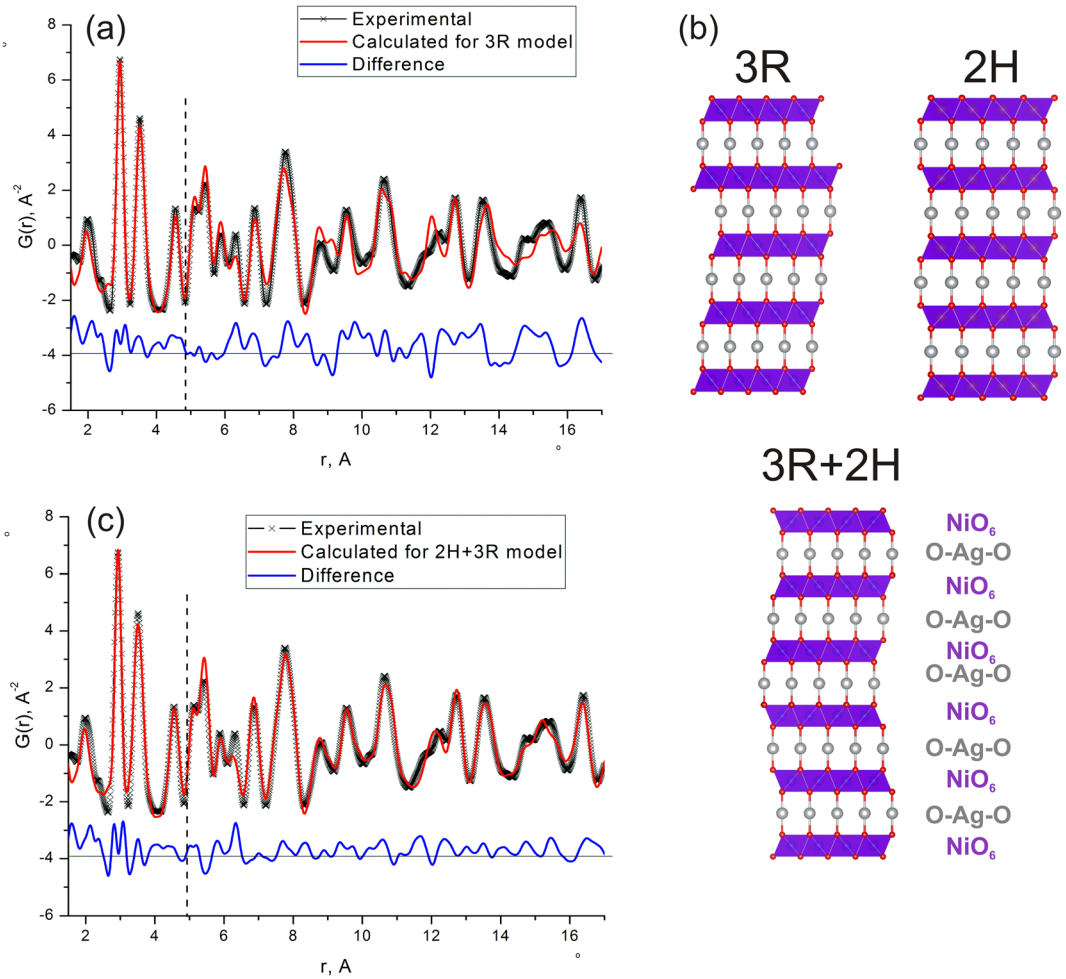

Fig. 1 (a) Comparison of the experimental PDF curve for the initial oxide $AgNiO_2$ with the calculated curve for the stoichiometric delafossite structure of 3R polytype (R = 0.32). (b) Polytypes of a delafossite structure: 2H, 3R and defect structure with alternating 2H and 3R layers. (c) Comparison of the experimental PDF curve with the calculated curve for the simulated structure with alternating 2H and 3R layers (R = 0.25).

compounds with a predominantly divalent character of nickel (Fig. S3, ESI†). It emphasizes that the analysis of shake-up satellite structures may be considered as the most reliable approach for the detection of Ni^{3+} species. To analyze the intensity of satellites, we used the F(Ni) parameter calculated as the I_1(Ni $2p_{3/2}$)/I_2(shake-up) ratio (Fig. 2a). In the case of the initial $AgNiO_2$, the value of the F(Ni) parameter 2.6 ± 0.1 eV was noticeably higher than for the NiO (F(Ni) = 1.9) and $Ni(OH)_2$ (F(Ni) = 2.1) reference samples, indicating the presence of Ni^{3+} forms presumably in the low-spin state $t_{2g}^6e_g^1$.[14] However, the observed spectral characteristics (the Ni $2p_{3/2}$ peak with E_b of 854.6 eV, the structure of satellites in the region of 858–866 eV, Fig. 2a) did not correspond only to the state of Ni^{3+}. The observed pattern corresponds either to a combination of Ni^{2+} and Ni^{3+} forms, or to the oxidized nickel state with an average charge $+3-\delta$. Previously, the XAS data indicated the presence of Ni^{2+} forms (up to 60%) in addition to the Ni^{3+} species in the bulk of $AgNiO_2$ particles.[48] The authors explain this behavior by the higher stability of Ni^{2+} compared to low-spin Ni^{3+} in an octahedral (O_h) environment. The detection of Ni^{2+}/Ni^{3+} pair in the particle bulk does not exclude their presence on the surface, which may be revealed by a surface-sensitive XPS technique.

On the basis of both literature data and the obtained XPS results, we assumed the presence of a combination of Ni^{3+} and Ni^{2+} states on the pristine $AgNiO_2$ surface.

Silver on the $AgNiO_2$ surface was characterized by the position of the Ag $3d_{5/2}$ peak at 367.8 eV, while modified Auger-parameter α'(Ag) calculated as a sum of binding energy (E_b) for the Ag $3d_{5/2}$ peak and kinetic energy (E_{kin}) for Ag $M_4N_{45}N_{45}$ maximum was close to 725.2 ± 0.1 eV (Fig. S4, ESI†). Note that Wedig *et al.*[47] showed that the value of E_b(Ag $3d_{5/2}$) for $AgNiO_2$ was close to 367.7 eV, which is close to the result of the current work. Based on the position of E_b(Ag $3d_{5/2}$), the authors considered the state of silver in $AgNiO_2$ as the oxidized monovalent form (Ag^+).

However, the observed value of α'(Ag) equal to 725.2 ± 0.1 eV is not typical for monovalent silver. For example, for Ag_2O oxide, the α'(Ag) value is usually close to 724.5 eV,[51,52] while for ionic silver compounds, the Auger parameter is usually lower than 724 eV.[53,54] Note that for deeply oxidized silver in an

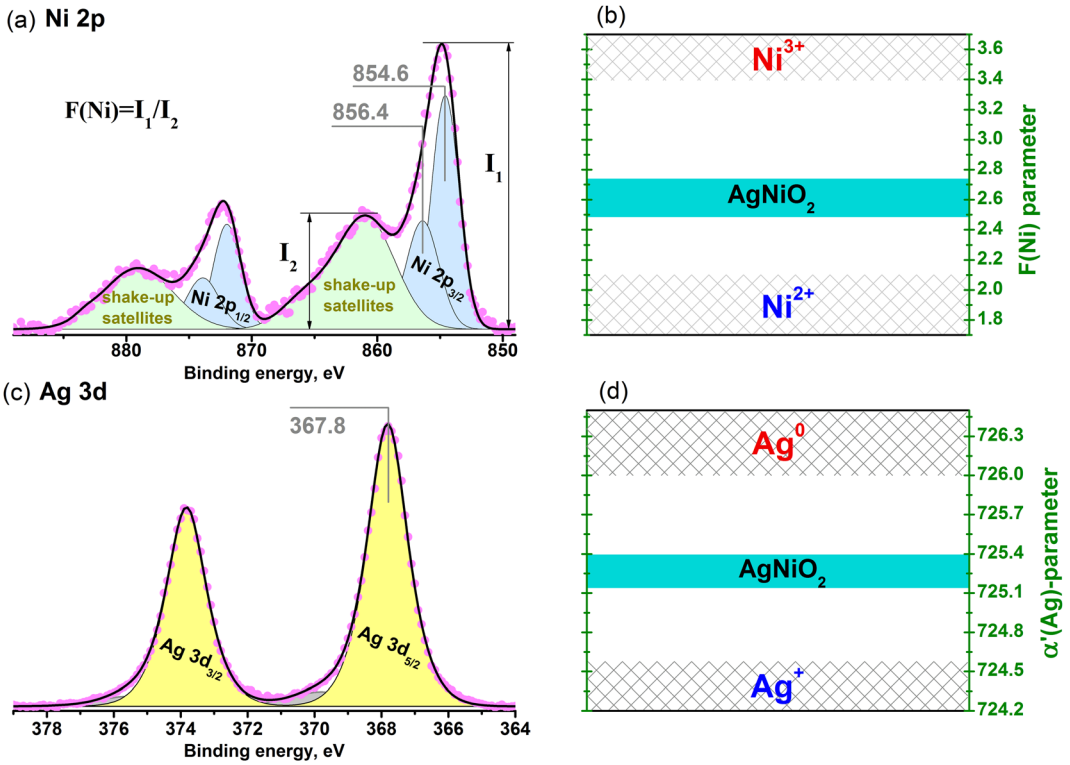

Fig. 2 (a) Ni 2p and (c) Ag 3d photoelectron spectra for the initial $AgNiO_2$ sample and corresponding diagrams for the (b) *F*(Ni) and (d) α'(Ag) parameters.

oxygen environment (AgO-like), the value of α'(Ag) is also close to 724.7 eV.[51,53] The value of α'(Ag) above 725 eV is usually explained by the contribution of metallic silver, for which the Auger parameter is >726 eV.[51–53]

For $AgNiO_2$, the position of the Ag $3d_{5/2}$ peak and corresponding half-width value (FWHM = 1.4 eV) indicated the presence of a single state of silver, but not a combination of Ag^+ and Ag^0. This state of silver on the surface of $AgNiO_2$ is unusual due to the more covalent (less ionic) nature of the bond with oxygen than silver in Ag_2O or AgO oxides. Our results are consistent with the conclusion about the strong interaction between silver and oxygen in $AgNiO_2$, which was made on the basis of spectral data and DFT calculations.[47]

The O 1s spectrum for the initial $AgNiO_2$ was a superposition of three components with peak binding energies of 529.0, 531.0, and 533.3 eV attributed to Ag–O–Ni lattice oxygen, surface oxygen and adsorbed molecules (CO_x, H_2O), respectively (Fig. S5a, ESI†). The component with E_b(O 1s) = 531.0 eV with a high half-width value (FWHM = 2.3 eV) is a combination of O-containing species with similar binding energies, which are hard-to-distinguish: (1) impurity carbonates/hydrocarbonates,[53,55] (2) hydroxyl groups,[56] (3) active weakly charged oxygen with E_b(O 1s) $\sim$ 530 eV, capable of interacting with CO at room temperature,[14] and (4) other possible forms of chemisorbed oxygen, including associative species.[20–23,27,28] The example of the curve-fitting of the O 1s spectrum by more than 3 components and interpretation are presented in Fig. S5b (ESI†).

A partially reduced $AgNiO_2$ surface or the presence of oxygen vacancies can be a reason for the decrease in silver and nickel average charge compared to those of Ag^{1+} and Ni^{3+}. The O/(Ag + Ni) ratio according to XPS data for the as-synthesized sample was 0.98 (Table S2, ESI†). Taking into account the initially low silver concentration (Ag/Ni $\sim$ 0.7), as well as surface impurities on the oxide surface (CO_3^{2-}/HCO_3^{2-} or OH^-/H_2O), the O/(Ag + Ni) ratio should be noticeably higher than 1, as was observed for other similar oxides.[34,35,39] Based on such considerations, it can be concluded that the initial $AgNiO_2$ surface is partially reduced. This may be due to the high reactivity of $AgNiO_2$ at room temperature.[14] However, prolonged air-storage did not result in any significant changes of Ni and Ag states on the $AgNiO_2$ surface (Fig. S6, ESI†). No evident presence of S- and Na-containing species was found by XPS on the surface of the as-prepared $AgNiO_2$ particles (Fig. S7, ESI†).

Interaction with ethylene: *Ex situ* XPS

The epoxidation ability of silver catalysts is usually associated with the presence of electrophilic oxygen species with the covalent nature of the Ag–O bond.[27,57,58] At the same time, the surface of silver particles is partially oxidized under the reaction conditions, providing efficient adsorption of alkenes.[31,59] The states of nickel (Ni^{3+}) and silver ($Ag^{\delta+}$) on the $AgNiO_2$ surface should stabilize highly reactive oxygen species.[14] The increased covalent character of the Ag–O bond for $AgNiO_2$ in comparison with AgO_x oxides (x = 0.5 and 1) causes interest in its application for selective oxidation reactions, for example, epoxidation.

Fig. 3 shows the O 1s spectra measured before and after the interaction of $AgNiO_2$ oxide with ethylene (10^{11} L exposure) in

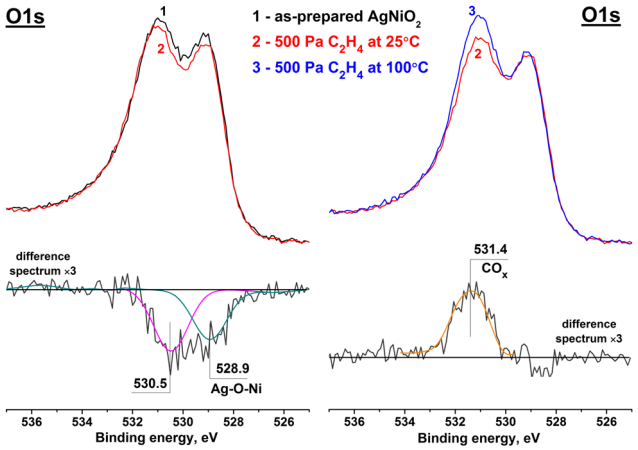

Fig. 3 Normalized O 1s spectra for the $AgNiO_2$ sample before and after interaction with 500 Pa of C_2H_4 at 25 and 100 °C.

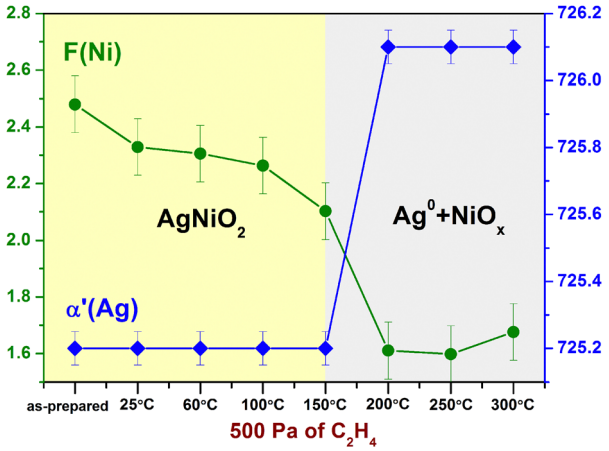

Fig. 4 Evolution of the F(Ni) and α'(Ag) parameters for $AgNiO_2$ oxide as a result of the interaction with ethylene at temperatures from 25 to 300 °C.

the preparation chamber of a photoelectron spectrometer without being exposed to air. During the experiment, the sample was sequentially heated in an ethylene atmosphere (P = 500 Pa) at temperatures in the range from 25 to 300 °C. The most noticeable changes were observed after interaction at room temperature: two components with E_b(O 1s) = 528.9 eV and 530.5 eV were removed (difference spectrum, Fig. 3). With an increase in temperature to 60–100 °C, the titration of reactive oxygen species was accompanied by the accumulation of a noticeable number of carbon-containing species with E_b(C 1s) = 285.1 and 288.2 eV assigned to C–C forms and oxidized carbon, respectively (Fig. S8, ESI†). In this case, the O 1s signal from lattice oxygen in the region of 528–530 eV was not changed. When heated up to 150 °C, no significant changes in the O 1s spectrum were observed, while at 200 °C a shift of the lattice oxygen O 1s peak towards higher binding energies was detected (Fig. S9, ESI†). The shift increased with rising temperature and reached 0.7 eV at 300 °C. This shift is associated with the destruction/reorganization of the initial surface structure and the formation of more covalent bonds between metals and oxygen. This was accompanied by a decrease in the O/(Ag + Ni) value from ~0.97 (at 150 °C) to 0.57 (at 200 °C) and then to 0.41 (at 300 °C). The quantitative ratios of elements on the surface of $AgNiO_2$ as a result of interaction with ethylene are presented in Table S1 (ESI†).

To analyze the electronic states of nickel and silver during the interaction with ethylene, we followed the change in the F(Ni) and α'(Ag) parameters depending on the reaction temperature (Fig. 4). The interaction at room temperature resulted in a slight decrease in the F(Ni) parameter to 2.3 (Fig. 4) without a noticeable change in the silver state (α'(Ag) = 725.2 eV). The drop in the F(Ni) value is associated with the partial reduction of Ni^{3+} to Ni^{2+} on the oxide surface, probably due to the removal of reactive oxygen species (Fig. 3). Significant changes in the F(Ni) and α'(Ag) parameters occurred at T > 150 °C: (1) the value of F(Ni) dropped to 1.6 due to an increase in the intensity of shake-up satellites (Fig. S10, ESI†); (2) the α'(Ag) value increased to 726.1 eV indicating the transformation to metallic silver.[53] This is due to the complete destruction of the delafossite structure as a result of the reduction of the Ni^{3+} and $Ag^{\delta+}$ forms to Ni^{2+} and Ag^0, respectively. Presumably, particles of metallic silver (Ag^0) and oxidized nickel (NiO_x) were formed.

Interaction with ethylene: Flow reactor

Fig. 5 shows the results of $AgNiO_2$ testing in ethylene epoxidation at room temperature (a and b) and at subsequent heating up to 200 °C (c and d). At room temperature, ethylene conversion was close to 5%. Most of the ethylene was oxidized to ethylene oxide (EtO) with a selectivity of about 70%, while the CO_2 selectivity was 30%. The selectivity for acetaldehyde (AcA) was within the quantitative error (<5%). Ethylene conversion at 5% was observed for 2500 seconds, followed by a drop in sample activity.

The observed deactivation might be caused by the removal of reactive oxygen species and/or the accumulation of strongly bounded surface species. The part of oxygen extracted from $AgNiO_2$ during the interaction with ethylene at 20 °C up to the drop in catalytic activity was estimated to be close to 3%. This calculation was made when comparing the molar quantity of the sample loaded into the reactor with the total amount of oxidized ethylene during the catalytic measurement. Subsequent heating above 50 °C led to an increase in ethylene conversion of up to 6%, which was accompanied by a noticeable drop in the selectivity for ethylene oxide down to 15% (Fig. 5c and d). This is consistent with *ex situ* XPS data on the appearance of carbonate-like oxygen species with E_b(O 1s) = 531.5 eV after interaction with ethylene at 100 °C (Fig. 3). Above 150 °C, a noticeable increase in ethylene conversion of up to 15% was observed. In this case, the selectivity for ethylene oxide decreased to 4%, and CO_2 was the main product.

Observed changes in conversion/selectivity values were associated with structural transformations in the sample. In particular, according to XRD data, after heating of $AgNiO_2$ in a $C_2H_4 + O_2$ atmosphere at 200 °C, the appearance of the Ag^0 phase was detected (reflections at $2\theta = 38.1°$ and 44.3°, ICDD PDF-200-004-0783, Fig. S1, ESI†). Note that the complete destruction of the delafossite structure did not occur in this case. According to

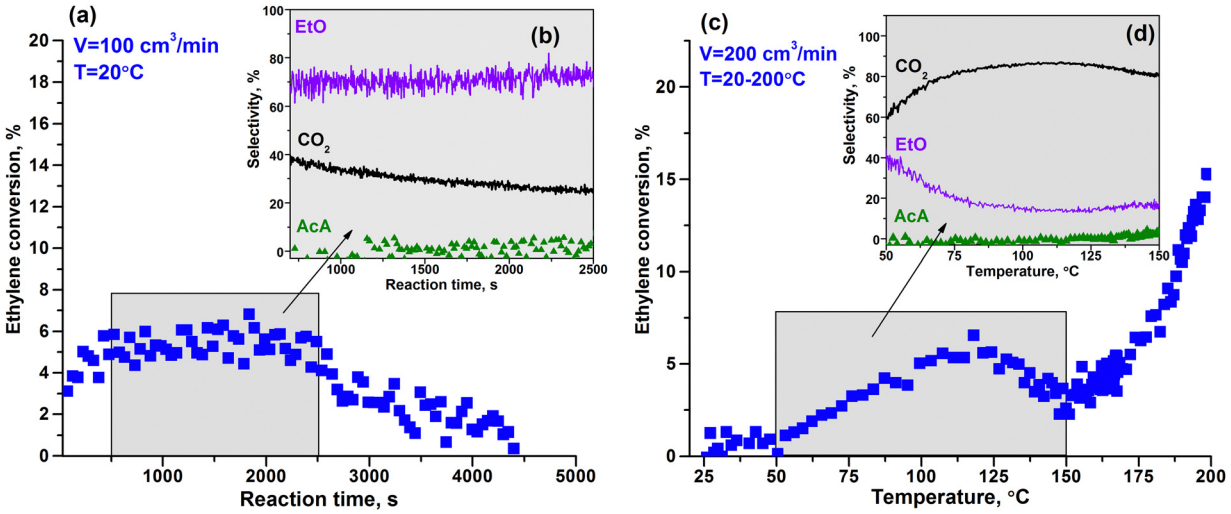

Fig. 5 Ethylene conversion and selectivity for ethylene oxidation products for the $AgNiO_2$ sample at 20 °C (a) and (b) and during subsequent heating to 200 °C (c) and (d) in a 2.5%C_2H_4/5%O_2/He mixture.

in situ XRD data, the delafossite structure was completely destroyed only when heated in a C_2H_4 + O_2 mixture at $T \geq 250$ °C (Fig. S11a, ESI†).

The coexistence of the $AgNiO_2$ phase and Ag^0 particles formed at 150–200 °C may be due to the accumulation of cationic vacancies in silver positions of the delafossite structure. It is known that delafossite $AgBO_2$ can accommodate up to 15% of vacancies in the silver positions. Charge compensation is implemented through the additional oxidation of B cations.[60,61] According to the PDF, the interaction of $AgNiO_2$ with the reaction mixture at 20 °C did not cause noticeable structural changes, except for small deviations in the range of interlayer distances (5–5.5 Å, Fig. 6a). This may be related to the redistribution of cations in the interlayer space, for example, the diffusion of silver ions from the bulk to the surface/subsurface zone. After heating at 200 °C in a C_2H_4 + O_2 mixture, additional peaks corresponding to interatomic distances in Ag^0 particles were observed on the PDF curve, while peaks of the delafossite structure were preserved (Fig. 6b).

Thus, the initial surface of $AgNiO_2$ was characterized by the presence of oxygen species capable of interacting with ethylene at room temperature. The main product of this interaction was ethylene oxide ($S_{EtO} \sim 70\%$). The interaction of $AgNiO_2$ with the reaction medium at 20 °C caused small structural changes due to the redistribution of silver ions in the interlayer space, while heating in a reaction medium of up to 200 °C resulted in the partial release of silver from the delafossite structure without destroying the latter.

Temperature-programmed reduction (TPR)

Fig. 7 shows the TPR-C_2H_4 curves for the as-prepared $AgNiO_2$ sample before and after pretreatment in O_2 at 200 °C. For the pristine $AgNiO_2$ sample, two main reduction peaks were observed with maxima at 245 °C (transition of $AgNiO_2$ to Ag^0 and NiO_x) and 365 °C (reduction of NiO_x to Ni^0). The integral molar ratio of $CO_2/AgNiO_2$ as a result of interaction with C_2H_4 was close to 0.9 for the overall temperature range, which is consistent with the reduction of $AgNiO_2$ oxide to metallic silver

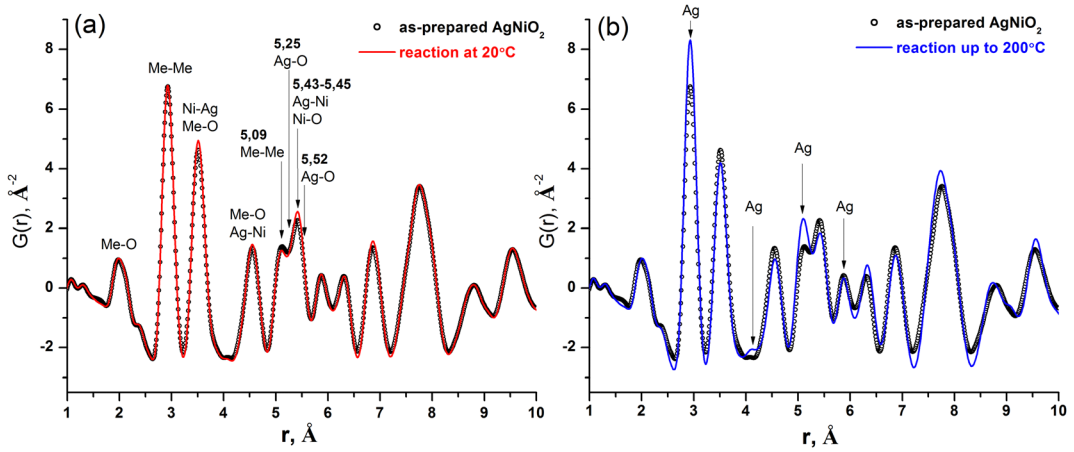

Fig. 6 Comparison of the PDF curves for $AgNiO_2$ before and after interaction with a reaction mixture (a) at 20 °C and (b) after heating to 200 °C.

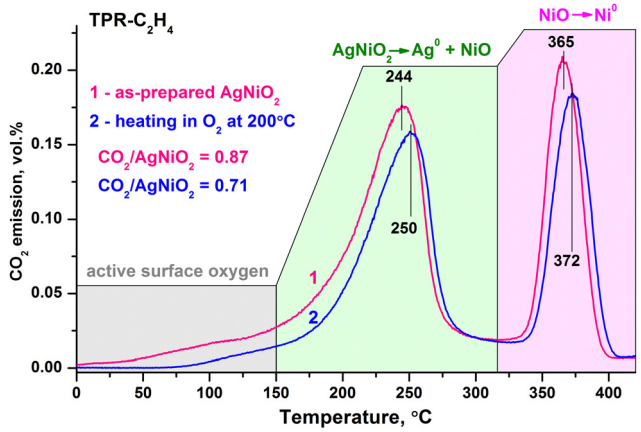

Fig. 7 TPR-C_2H_4 curves of $AgNiO_2$ before and after pretreatment in 20%O_2/He at 200 °C.

and nickel. Also, the corresponding TPR curve was characterized by a noticeable shoulder in the range from 0 to 150 °C, which indicated the presence of reactive surface oxygen species. The relative abundance of such species was close to 8.5%. Pretreatment of $AgNiO_2$ in an O_2 flow at 200 °C resulted in the partial removal of reactive oxygen (the relative amount dropped down to 3%) and a shift in the main reduction peaks towards higher temperatures (by 6–7 °C).

Note that this pretreatment did not cause destruction of the delafossite structure (Fig. S11b, ESI†). In this case, the CO_2/$AgNiO_2$ molar ratio decreased to 0.7 for the treated $AgNiO_2$ sample due to the removal of both reactive surface oxygen and a decrease in the intensity of the main peaks in the TPR curve. This indicates equilibrium between the reactive surface and lattice oxygen species in $AgNiO_2$. This conclusion was supported by XPS data, which showed that both lattice and surface weakly charged oxygen species were removed simultaneously by ethylene. Thus, surface reactive oxygen species (peaks up to 150 °C on the TPR-C_2H_4 curve) might be related to weakly charged oxygen (E_b(O 1s) = 530.5 eV, Fig. 3). Note that weakly charged oxygen with similar characteristics exhibit electrophilic properties during the epoxidation of ethylene.[27,57,58]

The presented TPR-C_2H_4 data demonstrate the relatively low thermal stability of reactive oxygen species on the $AgNiO_2$ oxide surface. Most of these forms were removed by heating in an O_2-containing mixture at 200 °C. At the same time, lattice oxygen of $AgNiO_2$ may be removed only in the temperature range of 300–400 °C (TPD-He study, Fig. S12, ESI†). Note also that a two-step process of $AgNiO_2$ reduction as well as the presence of active surface oxygen with reactivity at $T < 75$ °C were also observed during the TPR-H_2 study (Fig. S13, ESI†).

Discussion

Oxygen forms and silver electronic state on the $AgNiO_2$ surface

Two oxygen species, which react with ethylene, with E_b(O 1s) = 529.0 and 530.5 eV (Fig. 3) were found on the surface of $AgNiO_2$ oxide. These species can be considered as nucleophilic and electrophilic forms of oxygen, respectively. As a result of the $AgNiO_2$ interaction with ethylene at room temperature, high selectivity for ethylene oxide was observed (~70%), which may be due to the presence of electrophilic oxygen with E_b(O 1s) = 530.5 eV.[26–30] Nucleophilic oxygen with E_b(O 1s) = 529.0 eV is the lattice oxygen (Ag–O–Ni) of the delafossite structure.[14] Note that the stabilization of electrophilic oxygen with epoxidation activity is due to the defect structure of delafossite and the specific electronic states of Ni and Ag species on the surface. According to XPS and literature data,[48] nickel on the $AgNiO_2$ surface is represented by a combination of Ni^{2+} and Ni^{3+} states (Fig. 2a and b). Silver on the surface of $AgNiO_2$ is represented by single oxidized state with the α'(Ag) parameter close to 725.2 eV (Fig. 2d). This value is intermediate between metallic (>726 eV) and oxidized silver in Ag_2O or AgO oxides (724.5–724.7 eV).[51,53] Based on the α'(Ag) value, it was concluded that the Ag–O bond in $AgNiO_2$ is more covalent in comparison with that of individual AgO_x oxides. The stabilization of electrophilic oxygen on the $AgNiO_2$ surface is most likely associated with the formation of an oxygen bond with silver atoms in a state intermediate between Ag^0 and Ag^{1+}, *i.e.* $Ag^{\delta+}$ ($\delta < 1$).

According to literature data, the oxygen species with (E_b(O 1s) = 530.5 eV) is electrophilic oxygen.[26–30] Associative oxygen forms are the most likely candidates for this role on the surface of $AgNiO_2$, for example, peroxide (O_2^{2-}-like), superoxide (O_2^--like), or ozonide (O_3-like) oxygen. Note that the preparation of $AgNiO_2$ by co-precipitation was carried out in the presence of peroxodisulfate (see Section 2.1), and it could be a reason for the stabilization of peroxide or superoxide forms on the $AgNiO_2$ surface. Electrophilic oxygen with epoxidation activity in the form of ozonide species on the surface of silver particles is discussed elsewhere.[26,27,62] At the same time, the appearance of such forms is associated with the presence of cationic vacancies on the reconstructed silver surface.[26] The presence of vacancies in the positions of silver cations in the $AgNiO_2$ structure was noted based on PDF data (Fig. 1) and XPS results (Ag/Ni < 1). This is also consistent with the literature data for similar materials.[60] In this case, the diffusion of surface oxygen to the Ni–O–[ ]–O–Ni vacancy sites can form ozonide-like species of oxygen like Ni–O–O–O–Ni. The limited diffusion rate at temperatures <100 °C may be the reason for the low efficiency of regeneration of such forms, leading to a decrease in the overall activity upon reaction time. However, a detailed study of the epoxidation oxygen on the $AgNiO_2$ surface requires a systematic study using modern experimental and theoretical research methods.

Nickel role

The improved epoxidation activity of mixed oxide $AgNiO_2$ at room temperature might be provided not only by silver species, but also by nickel sites. Nickel-modified silver catalysts are known to exhibit improved performance in the epoxidation reaction. For example, an increase in the Ni content leads to the formation of dispersed Ag particles with an optimal concentration of oxidized silver, which causes an increase in selectivity

for propylene epoxide.[63] It was established that the control of the Ag/Ni ratio during the synthesis of Ni@Ag core–shell structures makes it possible to optimize the Ag–Ag interatomic distance by varying the thickness of the silver shell.[64] In this case, an increase in selectivity to the epoxidation product was observed. Another possible role of nickel may be isolation of silver sites from each other, which reduces the efficiency of the complete oxidation route in accordance with the Grasselli concept.[4] However, Ni^{2+} complex compounds are active in epoxidation of olefins by molecular oxygen in liquid.[65] The presence of cationic vacancies in $AgNiO_2$ according to PDF and XPS (Ag/Ni $<$ 1) data indicates the potential for the presence of surface oxygen bounded directly to nickel atoms (Ni–O). Moreover, during the interaction of $AgNiO_2$ with ethylene up to 150 °C, the reduction of nickel on the surface was observed (a drop in the *F*-parameter), while the state of silver was found to be unchanged (Fig. 4). In accordance with TPR-C_2H_4, in the temperature range below 150 °C, reactive forms of surface oxygen were removed (Fig. 7). These data do not exclude the stabilization of electrophilic epoxidation oxygen, including on the nickel sites of the defective delafossite structure.

Active oxygen regeneration

Regeneration of reactive oxygen species when exposed to molecular oxygen in the gas phase is one of the most important for catalysis. In the case of a mixture of C_2H_4 + O_2 at 20 °C, a decrease in oxidative activity of $AgNiO_2$ was observed after 50 min of the reaction (Fig. 5a), which is most likely due to the removal of reactive oxygen species. Moreover, experiments carried out in a flow reactor both in the presence and absence of O_2 at room temperature showed similar results. This indicates that the active oxygen forms on the $AgNiO_2$ surface are not reproduced after interaction with O_2 at 20 °C. Therefore, the regeneration of active oxygen was studied at an elevated temperature (60 °C). Experiments were carried out at different atmospheres: (1) interaction with ethylene, (2) interaction with a C_2H_4 + O_2 mixture, and (3) successive interaction with C_2H_4, and then with O_2. Details of such experiments are presented in ESI† (Fig. S14–S16). When comparing the difference O 1s spectra obtained in the absence (experiment 1) and in the presence (experiments 2 and 3) of molecular oxygen, differences were revealed (Fig. S14, ESI†). When $AgNiO_2$ was treated only with ethylene at 60 °C, removal of oxygen species with E_b(O 1s) = 528.6 and 530.0 eV was observed, as well as the accumulation of carbonate-like groups with E_b(O 1s) = 531.5 eV was detected. In the presence of O_2 during the interaction at 60 °C, the difference in O 1s spectra showed only the accumulation of carbonates. This result indirectly indicates the possibility of regeneration of reactive oxygen species on the $AgNiO_2$ surface upon interaction with O_2 at 60 °C. However, the efficiency of this process might be insufficient due to kinetic limitations, resulting in a drop in overall epoxidation activity with reaction time. Additionally, a TPO study was performed for $AgNiO_2$ preliminary treated with ethylene at 30 °C for more than 1 h (Fig. S17, ESI†). The O_2 consumption was observed in temperature ranges of 20–100 °C and 120–180 °C indicating the possibility of O_2 activation on the $AgNiO_2$ surface.

Conclusions

Mixed oxide $AgNiO_2$ was prepared by co-precipitation in an alkaline solution in the presence of peroxodisulfate. As a result, highly dispersed particles with a delafossite type structure were obtained. According to the PDF method, the initial structure of $AgNiO_2$ was characterized by the presence of stacking faults, as well as cationic vacancies at silver positions, which determined the mobility of such cations in the interlayer space and oxide nonstoichiometry (Ag/Ni $<$ 1). On the surface of $AgNiO_2$, silver had a more covalent (less ionic) bond with oxygen than in individual silver oxides. The unusual electronic states of silver and nickel, together with the developed defect structure of $AgNiO_2$ oxide, cause the appearance of reactive oxygen species including oxygen with E_b(O 1s) = 530.5 eV, which was able to react with ethylene at room temperature. It has been established that this interaction is accompanied by the formation of ethylene oxide with selectivity close to 70% for about 50 min. An increase in the reaction temperature of up to 150 °C leads to the efficient oxidation of ethylene predominantly to CO_2 (the selectivity with respect to EtO is no more than 20%). *In situ* XRD and PDF studies revealed that the interaction of $AgNiO_2$ with the reaction mixture at room temperature did not cause noticeable structural transformations, except for the redistribution of cations in the interlayer space. At 150–200 °C, the formation of metallic silver particles was observed with the preservation of delafossite-type structure. Above 200 °C, this structure was completely destroyed with the formation of an Ag^0/NiO composite. According to the TPR-C_2H_4 data, the relative amount of weakly bounded and reactive oxygen on the $AgNiO_2$ surface reached 8.5 at%, while no more than 3% of oxygen was involved in ethylene epoxidation at room temperature. In accordance with the obtained results and the literature data, oxygen with E_b(O 1s) $>$ 530 eV observed on the $AgNiO_2$ surface by XPS under vacuum conditions might be an associated species, which are considered as electrophilic oxygen directly involved in the epoxidation of ethylene.

Author contributions

Dmitry A. Svintsitskiy: conceptualization, writing – original draft, writing – review & editing, data curation, visualization, methodology, and validation. Mikhail K. Lazarev: investigation. Elena M. Slavinskaya: formal analysis, investigation, and writing – review & editing. Elizaveta A. Fedorova: investigation. Tatyana Yu. Kardash: formal analysis, writing – review & editing, visualization, and validation. Svetlana V. Cherepanova: formal analysis. Andrei I. Boronin: conceptualization, writing – review & editing, methodology, validation, and supervision.

Conflicts of interest

There are no conflicts to declare.

Acknowledgements

This work was supported by the Ministry of Science and Education of the Russian Federation within the framework of the budget project of the Boreskov Institute of Catalysis (project AAAA-A21-121011390053-4). Experiments on a photoelectron spectrometer were performed using the equipment of the ''National Center for the Study of Catalysts''.

Notes and references

1 Y. Pu, Y. Liu, D. Liu, Z. Zhou, S. Ding, Z. Xia and M. Li, *Int. J. Hydrogen Energy*, 2018, **43**, 17271–17282.
2 H. Wang, K. H. L. Zhang, J. P. Hofmann, V. A. de la Peña O'Shea and F. E. Oropeza, *J. Mater. Chem. A*, 2021, **9**, 19465–19488.
3 J. C. Vedrine, *J. Energy Chem.*, 2016, **25**, 936–946.
4 R. K. Grasselli, *Catal. Today*, 2014, **238**, 10–27.
5 W. C. Sheets, E. Mugnier, A. Barnabe, T. J. Marks and K. R. Poeppelmeier, *Chem. Mater.*, 2006, **18**, 7–20.
6 D. Muñoz-Rojas, G. Subías, J. Oró-Solé, J. Fraxedas, B. Martínez, M. Casas-Cabanas, J. Canales-Vázquez, J. Gonzalez-Calbet, E. García-González, R. I. Walton and N. Casañ-Pastor, *J. Solid State Chem.*, 2006, **179**, 3883–3892.
7 C. Martin and M. Poienar, *J. Cryst. Growth*, 2017, **472**, 71–75.
8 M. A. Marquardt, N. A. Ashmore and D. P. Cann, *Thin Solid Films*, 2006, vol. 496, pp. 146–156.
9 T. I. Draskovic and Y. Wu, *ChemCatChem*, 2017, **9**, 3837–3842.
10 D. A. Svintsitskiy, V. M. Metalnikova, S. V. Cherepanova and A. I. Boronin, *J. Struct. Chem.*, 2022, **63**, 1496–1508.
11 M. H. Whangbo, D. Dai, K. S. Lee and R. K. Kremer, *Chem. Mater.*, 2006, **18**, 1268–1274.
12 Y. Zhao, H. An, G. Dong, J. Feng, T. Wei, Y. Ren and J. Ma, *Chem. Eng. J.*, 2020, **388**, 124371.
13 D. A. Svintsitskiy, T. Y. Kardash, E. A. Fedorova, E. M. Slavinskaya and A. I. Boronin, *Appl. Surf. Sci.*, 2020, **525**, 1–10.
14 D. A. Svintsitskiy, M. K. Lazarev, T. Y. Kardash, E. A. Fedorova, E. M. Slavinskaya and A. I. Boronin, *J. Chem. Phys.*, 2020, **152**, 044707.
15 T. Pu, H. Tian, M. E. Ford, S. Rangarajan and I. E. Wachs, *ACS Catal.*, 2019, 10727–10750.
16 J. G. Serafin, A. C. Liu and S. R. Seyedmonir, *J. Mol. Catal. A: Chem.*, 1998, **131**, 157–168.
17 M. A. Salaev, A. A. Salaeva and O. V. Vodyankina, *Catal. Today*, 2021, **375**, 585–590.
18 V. V. Torbina, A. A. Vodyankin, S. Ten, G. V. Mamontov, M. A. Salaev, V. I. Sobolev and O. V. Vodyankina, *Catalysts*, 2018, **8**, 447.
19 S. Rebsdat and D. Mayer, *Ullmann's encyclopedia of industrial chemistry*, Wiley-VCH, New York, 2012, pp. 547–572.
20 Z. Tang, T. Chen, K. Liu, H. Du and S. G. Podkolzin, *Langmuir*, 2021, **37**, 11603–11610.
21 C. Liu, D. P. Wijewardena, A. Sviripa, A. Sampath, D. W. Flaherty and C. Paolucci, *J. Catal.*, 2022, **405**, 445–461.
22 H. A. Alzahrani and J. J. Bravo-Suárez, *J. Catal.*, 2023, **418**, 225–236.
23 T. Pu, A. Setiawan, B. Mosevitzky Lis, M. Zhu, M. E. Ford, S. Rangarajan and I. E. Wachs, *ACS Catal.*, 2022, **12**, 4375–4381.
24 V. I. Bukhtiyarov, A. I. Nizovskii, H. Bluhm, M. Hävecker, E. Kleimenov, A. Knop-Gericke and R. Schlögl, *J. Catal.*, 2006, **238**, 260–269.
25 M. O. Özbek and R. A. Van Santen, *Catal. Lett.*, 2013, **143**, 131–141.
26 V. I. Avdeev, A. I. Boronin, S. V. Koscheev and G. M. Zhidomirov, *J. Mol. Catal. A: Chem.*, 2000, **154**, 257–270.
27 A. I. Boronin, S. V. Koscheev, K. T. Murzakhmetov, V. I. Avdeev and G. M. Zhidomirov, *Appl. Surf. Sci.*, 2000, **165**, 9–14.
28 L. S. Kibis, V. I. Avdeev, S. V. Koscheev and A. I. Boronin, *Surf. Sci.*, 2010, **604**, 1185–1192.
29 V. I. Bukhtiyarov, A. I. Boronin and V. I. Savchenko, *Surf. Sci.*, 1990, **232**, L205–L209.
30 T. C. R. Rocha, M. Hävecker, A. Knop-Gericke and R. Schlögl, *J. Catal.*, 2014, **312**, 12–16.
31 V. I. Bukhtiyarov, A. I. Boronin and V. I. Savchenko, *J. Catal.*, 1994, **150**, 262–267.
32 V. I. Bukhtiyarov, M. Hävecker, V. V. Kaichev, A. Knop-Gericke, R. W. Mayer and R. Schlögl, *Phys. Rev. B: Condens. Matter Mater. Phys.*, 2003, **67**, 2354221.
33 S. M. Hosseini, H. Hosseini-Monfared, V. Abbasi and M. R. Khoshroo, *Inorg. Chem. Commun.*, 2016, **67**, 72–79.
34 D. A. Svintsitskiy, T. Y. Kardash, E. M. Slavinskaya, O. A. Stonkus, S. V. Koscheev and A. I. Boronin, *Appl. Surf. Sci.*, 2018, **427**, 363–374.
35 D. A. Svintsitskiy, N. A. Sokovikov, E. M. Slavinskaya, E. A. Fedorova and A. I. Boronin, *J. Struct. Chem.*, 2022, **63**, 1723–1733.
36 X. Yang, S. Kattel, K. Xiong, K. Mudiyanselage, S. Rykov, S. D. Senanayake, J. A. Rodriguez, P. Liu, D. J. Stacchiola and J. G. Chen, *Angew. Chem., Int. Ed.*, 2015, **54**, 11946–11951.
37 D. A. Svintsitskiy, E. M. Slavinskaya, T. Y. Kardash, V. I. Avdeev, B. V. Senkovskiy, S. V. Koscheev and A. I. Boronin, *Appl. Catal., A*, 2016, **510**, 64–73.
38 D. A. Svintsitskiy, L. S. Kibis, D. A. Smirnov, A. N. Suboch, O. A. Stonkus, O. Y. Podycheva, A. I. Boronin and Z. R. Ismagilov, *Appl. Surf. Sci.*, 2018, **435**, 1273–1284.
39 D. A. Svintsitskiy, T. Y. Kardash and A. I. Boronin, *Appl. Surf. Sci.*, 2019, **463**, 300–309.
40 G. Ashiotis, A. Deschildre, Z. Nawaz, J. P. Wright, D. Karkoulis, F. E. Picca and J. Kieffer, *J. Appl. Crystallogr.*, 2015, **48**, 510–519.
41 P. Juhás, T. Davis, C. L. Farrow and S. J. L. Billinge, *J. Appl. Crystallogr.*, 2013, **46**, 560–566.
42 C. L. Farrow, P. Juhas, J. W. Liu, D. Bryndin, E. S. Boin, J. Bloch, T. Proffen and S. J. L. Billinge, *J. Phys.: Condens. Matter*, 2007, **19**, 335219.
43 S. Lowell, J. E. Shields, M. A. Thomas and M. Thommes, *Characterization of Porous Solids and Powders: Surface Area, Pore Size and Density*, 2006.

44 S. Böcklein, S. Günther, R. Reichelt, R. Wyrwich, M. Joas, C. Hettstedt, M. Ehrensperger, J. Sicklinger and J. Wintterlin, *J. Catal.*, 2013, **299**, 129–136.
45 V. I. Korsounski, R. B. Neder, K. Hradil, C. Barglik-Chory, G. Müller and J. Neuefeind, *J. Appl. Crystallogr.*, 2003, **36**, 1389–1396.
46 J. L. Durham, A. B. Brady, C. A. Cama, D. C. Bock, C. J. Pelliccione, Q. Zhang, M. Ge, Y. R. Li, Y. Zhang, H. Yan, X. Huang, Y. Chu, E. S. Takeuchi, K. J. Takeuchi and A. C. Marschilok, *Phys. Chem. Chem. Phys.*, 2017, **19**, 22329–22343.
47 U. Wedig, P. Adler, J. Nuss, H. Modrow and M. Jansen, *Solid State Sci.*, 2006, **8**, 753–763.
48 J. S. Kang, S. S. Lee, G. Kim, H. J. Lee, H. K. Song, Y. J. Shin, S. W. Han, C. Hwang, M. C. Jung, H. J. Shin, B. H. Kim, S. K. Kwon and B. I. Min, *Phys. Rev. B: Condens. Matter Mater. Phys.*, 2007, **76**, 195122.
49 A. F. Carley, S. D. Jackson, M. W. Roberts and J. O'Shea, *Surf. Sci.*, 2000, **454–456**, 141–146.
50 A. F. Carley, S. D. Jackson, J. N. O'Shea and M. W. Roberts, *Surf. Sci.*, 1999, **440**, L868–L874.
51 G. I. N. Waterhouse, G. A. Bowmaker and J. B. Metson, *Appl. Surf. Sci.*, 2001, **183**, 191–204.
52 A. I. Boronin, S. V. Koscheev and G. M. Zhidomirov, *J. Electron Spectrosc. Relat. Phenom.*, 1998, **96**, 43–51.
53 J. F. Moulder, W. F. Stickle, P. E. Sobol and K. D. Bomben, *Handbook of X-ray photoelectron spectroscopy*, PerkinElmer Corp, Eden Prairie, Minnesota, USA, 1992.
54 L. S. Kibis, D. A. Svintsitskiy, T. Y. Kardash, E. M. Slavinskaya, E. Y. Gotovtseva, V. A. Svetlichnyi and A. I. Boronin, *Appl. Catal., A*, 2019, **570**, 51–61.
55 C. D. Wagner, A. V. Naumkin, A. Kraut-Vass, J. W. Allison, C. J. Powell and C. J. Rumble, *Natl. Inst. Stand. Technol.*, Gaithersbg., 2003.
56 J.-C. Dupin, D. Gonbeau, P. Vinatier and A. Levasseur, *Phys. Chem. Chem. Phys.*, 2000, **2**, 1319–1324.
57 R. B. Grant and R. M. Lambert, *J. Catal.*, 1985, **92**, 364–375.
58 R. A. Van Santen and H. P. C. E. Kuipers, *Adv. Catal.*, 1987, **35**, 265–321.
59 Y. Lei, F. Mehmood, S. Lee, J. Greeley, B. Lee, S. Seifert, R. E. Winans, J. W. Elam, R. J. Meyer, P. C. Redfern, D. Teschner, R. Schlögl, M. J. Pellin, L. A. Curtiss and S. Vajda, *Science*, 2010, **328**, 224.
60 S. Kato, N. Takagi, K. Saito and M. Ogasawara, *ACS Omega*, 2019, **4**, 9763–9768.
61 Y.-J. Shin, J.-H. Kwak and S. Yoon, *Bull. Korean Chem. Soc.*, 1997, **18**, 775–778.
62 N. Kenge, S. Pitale and K. Joshi, *Surf. Sci.*, 2019, **679**, 188–195.
63 A. Takahashi, N. Hamakawa, I. Nakamura and T. Fujitani, *Appl. Catal., A*, 2005, **294**, 34–39.
64 B. Yu, T. Ayvalı, E. Raine, T. Li, M. M. J. Li, J. Zheng, S. Wu, A. A. Bagabas and S. C. E. Tsang, *Appl. Catal., B*, 2019, **243**, 304–312.
65 T. Mukaiyama and T. Yamada, *Bull. Chem. Soc. Jpn.*, 1995, **68**, 17–35.

